Development of a sustainable anti-washout soil-fly ash-slag-based geopolymer grout for offshore scour protection

Deepak Patwa[1], *Zihan* Sang[1], *Deepesh* Bansal[1], and *Kai* Yao[1,2,3*]

[1] Shenzhen Research Institute of Shandong University, Shenzhen 518057, China
[2] School of Qilu Transportation, Shandong University, Jinan 250002, China
[3] Xinjiang Research Institute of Shandong University, Changji 831100, China

Abstract. This study aims to develop an anti-washout geopolymer grout using dredged river sediments (DRS), fly ash (FA), and ground granulated blast-furnace slag (GGBS) to mitigate scour around offshore structure foundations. The anti-washout soil-FA-GGBS (AWSFG) grout consisted of 70% DRS and 30% FA-GGBS (1:1), activated with sodium silicate solution and NaOH, and modified with 0.1% polyacrylamide (PAM) to improve washout resistance. The grout was prepared at a 1, 1.2, and 1.4 modulus value and 6%, 8%, and 10% Na_2O content. The performance of AWSFG grout was evaluated for fluidity, setting time, turbidity (anti-dispersion test), washout resistance, and unconfined compressive strength (UCS) at 3 days and 28 days curing periods. The AWSFG grout produces a fluidity in the range of 123-155 mm, exhibits a turbidity value between 16-62 NTU, minimum initial and final setting time of 105 and 227 minutes, washout resistance (97.84%-99.66%), and UCS values between 1.87 and 9.52 MPa. The results showed that the performance of AWSFG grout depends upon the modulus and Na_2O content. The sample M1.2N10 demonstrates optimum performance considering all parameters. Microstructural analysis revealed that the co-existence of ettringite, NASH, CASH, and CSH gel strengthens AWSFG grout. The properties of the AWSFG confirm its effectiveness as a robust anti-scouring grout.

1 Introduction

Offshore structures are large-scale engineering systems constructed in marine environments, including oceans, seas, rivers, and coastal regions. The stability of installations, including offshore wind turbine foundations, sea bridge piers, jacket structures, and oil and gas platforms, is strongly influenced by the strength and integrity of the surrounding seabed sediments. These foundations are persistently subjected to wave loading, tidal currents, and cyclic hydrodynamic actions, which can trigger localized seabed scour and significantly compromise structural safety [1, 2]. Consequently, improving the scour resistance of seabed sediments is a key measure for mitigating local scour damage. In this context, the development of cost-effective anti-scouring or anti-washout materials that can reinforce seabed soils under in-situ conditions has emerged as a promising solution [3].

Several studies have investigated scour protection for offshore wind turbines, using materials such as cement, sodium silicate, rubber powder, ionic soil stabilizers, and hydroxypropyl methylcellulose ether [3-5]. However, most of these studies used cement, often in combination with sodium silicate, as the primary binder. Cement production is environmentally detrimental, contributing approximately 10% of global CO_2 emissions, and its high alkalinity and carbon footprint adversely impact the geoenvironment [6]. Moreover, cement-stabilized soils exhibit limited durability under aggressive conditions, including chloride, sulfate, and acid exposure [7]. Therefore, there is a demanding need to develop sustainable, high-performance alternatives to Portland cement.

The geopolymerization offers the advantage of early high strength, excellent durability, corrosion resistance, high-temperature resistance, and decreased carbon footprint in comparison to cement [8, 9]. Moreover, it also provides exceptional resistance to deterioration driven by acids, sulfates, and chlorides that are typically present in wastewater and marine environments [10]. A recent study has explored soil-FA-GGBS-based geopolymer grout, using soil as the primary material and FA-GGBS as the binder for underwater applications [11]. However, the washout resistance of the grout declines at higher modulus and Na_2O content. Therefore, an investigation into the influence of modulus and Na_2O content, while maintaining a constant binder content, is needed. Further, there is also a need to improve the washout resistance of the grout.

This study aims to develop an anti-washout soil-FA-GGBS (AWSFG) grout using dredged river sediment (DRS), fly ash (FA), and ground granulated blast-furnace slag (GGBS), activated with sodium silicate solution and sodium hydroxide, and modified with 0.1% cationic polyacrylamide (PAM) to improve washout resistance. The alkali activator dosage was controlled by the silicate modulus (SiO_2/Na_2O molar ratio) and the

* Corresponding author: yaokai@sdu.edu.cn

Na_2O content (added as NaOH); thus, their effects were systematically investigated to identify optimal activation conditions. The AWSFG grout was evaluated in terms of fluidity, setting time, anti-dispersion behavior (turbidity), washout resistance, and unconfined compressive strength (UCS). Microstructural evolution and mineralogical characteristics of the hardened grout were examined using scanning electron microscopy (SEM) and X-ray diffraction (XRD) to elucidate the stabilization mechanism. By extensively utilizing DRS and industrial by-products (FA and GGBS), this low-cost and low-carbon grout demonstrates the potential of cement-free, alkali-activated materials for sustainable grouting applications.

2 Materials and methodology

2.1 Materials

The soil used in this study was a typical DRS collected from the Dehui River, Shandong, China. FA and GGBS were used as binders and were sourced from a fly ash plant and a titanium oxide plant in Jinan, Shandong, China. The specific gravity and Atterberg limits of DRS, FA, and GGBS were determined as per ASTM standards. The basic physical properties and particle size gradations are presented in Table 1 and Fig. 1, respectively.

Table 1. Basic properties of DRS, FA, and GGBS.

Properties	DRS (Soil)	Fly ash	GGBS
Specific gravity	2.71±0.02	1.66±0.05	2.82±0.02
Fine sand (425-75 μm)	8.14	6.24	0.33
Silt (75-2 μm)	90.62	91.73	95.5
Clay (< 2 μm)	1.24	2.03	4.17
Liquid limit (%)	31.2±1.2	35.3±1.2	58.0±1.2
Plastic limit (%)	19.2±1.1	23.3±1.2	36.1±1.0
Plasticity index (%)	12.0±1.1	12.00±1.1	21.9±1.0

The chemical compositions of DRS, FA, and GGBS, determined by X-ray fluorescence (XRF), are summarized in Table 2. The FA is classified as Class C fly ash, containing more than 20% CaO, along with 29.54% SiO_2 and 10.3% Al_2O_3 (39.84% combined). The GGBS comprises 31.05% CaO, 26.22% SiO_2, and 17.41% Al_2O_3. Thus, DRS, FA, and GGBS provide Si^{2+} and Al^{3+} ions, while FA and GGBS supply Ca^{2+}, making them suitable precursors for geopolymerization. An alkaline activator was prepared by combining sodium silicate solution and sodium hydroxide. The sodium silicate solution had a modulus of 3.3 and contained 8.37% Na_2O, 26.1% SiO_2, and 65.53% H_2O.

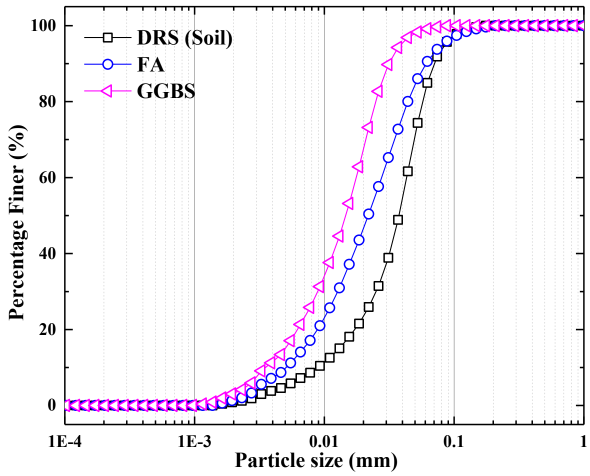

Fig. 1. Particle size distribution of DRS, FA, and GGBS.

Table 2. Basic properties of DRS, FA, and GGBS.

Major oxides (%)	DRS	FA	GGBS
SiO_2	62.78	29.54	26.22
Al_2O_3	12.41	10.30	17.41
CaO	7.06	25.45	31.05
Fe_2O_3	5.54	8.22	0.77
MgO	4.01	0.00	14.22
Na_2O	3.06	1.25	0.00
K_2O	2.66	5.18	0.35
TiO_2	0.87	1.20	0.80
CO_2	0.81	11.46	4.94
P_2O_5	0.32	2.19	0.00
ZrO_2	0.20	0.00	0.00
Cl	0.10	1.15	0.00
SrO	0.08	0.21	0.14
SO_3	0.00	3.61	3.85
Others	0.09	0.24	0.25

NaOH pellets with 96% purity were procured from MREDA, China. A cationic polyacrylamide (PAM) was used as an anti-washout admixture to improve the washout resistance of the alkali-activated slurry. The PAM had a molecular weight of 8-10 million. Fig. 2 shows the microstructural morphology of DRS, FA, and GGBS. DRS and GGBS particles exhibit irregular, blocky shapes, whereas FA particles are predominantly broken, angular, and highly irregular, with only a small fraction present as cenospheres. The details of the used material and alkali activator can be found in Patwa et al. [11, 12].

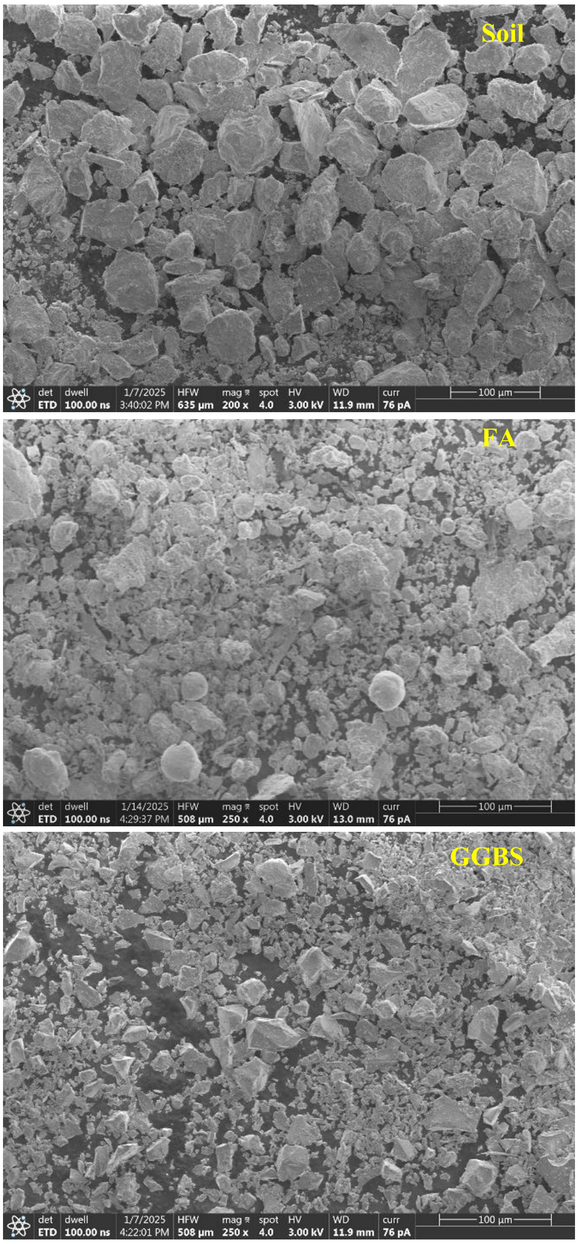

Fig. 2. SEM of Soil, FA, and GGBS.

2.2 Methodology

2.2.1 Experimental plan and sample preparation

The liquid limit of the DRS-FA-GGBS mix was determined as 34.57%. Based on this, the water-to-solid ratio was fixed at 0.5 (by weight), corresponding to approximately 1.5 times the liquid limit, to enable consistent evaluation of flowability, strength, and underwater performance of the AWSFG grout. The AWSFG grout was prepared as follows. First, alkali-activator solutions were prepared by mixing sodium silicate solution, NaOH powder, and distilled water using a spatula. The solutions were then stored for 1 day in a curing chamber maintained at 20 ± 2°C and 95% relative humidity to allow cooling and stabilization. Separately, dry DRS, FA, and GGBS were weighed and dry-mixed until a homogeneous blend was obtained. The cooled alkali-activator solution was then combined with the DRS-FA-GGBS mixture and mixed in a Hobart mixer at a slow speed for 2 minutes, followed by high speed for 3 minutes. Subsequently, PAM was added at a concentration of 0.1% (w/w) relative to the DRS-FA-GGBS content, and the grout was further mixed at a slow speed for 1 min, then at a high speed for 1 min to ensure uniform dispersion, yielding the AWSFG grout.

Chen et al. [13] reported that an alkaline activator modulus in the range of 1-1.4 is optimal for geopolymerization. Accordingly, this study adopted three modulus values (M = 1, 1.2, and 1.4) and three Na_2O contents (N = 6, 8, and 10% by weight of DRS-FA-GGBS). Previous studies indicate that Na_2O contents above 10% reduce compressive strength, whereas lower contents provide insufficient strength enhancement; therefore, 6%, 8%, and 10% were selected [14-16]. Sample designations such as M1N6, M1N8, and M1N10 denote mixes with a modulus of 1 and Na_2O contents of 6%, 8%, and 10%, respectively.

2.2.2 Fluidity, setting times, and anti-dispersion test

The fluidity of the grout samples was measured at room temperature in accordance with GB/T 8077-2023 [17]. The setting times of the slurry were determined using a Vicat apparatus following ASTM C191-21 [18]. The procedure for evaluating the anti-dispersion performance of the AWSFG grout is illustrated in Fig. 3. For this test, 500 g of fresh AWSFG grout was poured through a funnel with an internal diameter of 20 mm into a cubic container measuring 150×150×150 mm, with a vertical drop distance of approximately 40 mm between the funnel outlet and the container base. During pouring, the grout was eroded by water, causing partial particle dispersion and an increase in water turbidity. Immediately after pouring, water samples were collected from the center and other locations within the container to measure turbidity, which was used to evaluate the washout resistance of the grout. Higher turbidity values indicate lower resistance to erosion [9]. Turbidity was measured using a turbidity meter.

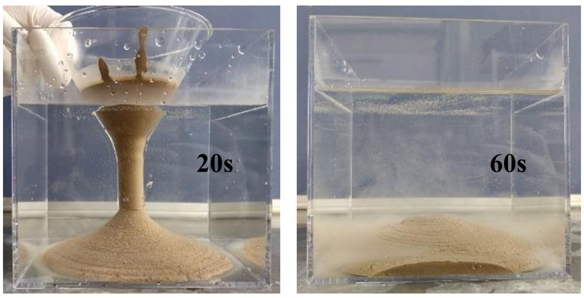

Fig. 3. Pouring of grout in water for anti-dispersion test.

2.2.3 Washout resistance test

Fig. 4 illustrates the experimental setup used to evaluate the washout resistance (WR) of the AWSFG grout. The setup consisted of a glass beaker, a rotor, and a petri dish. A mass of 50 g of fresh grout was placed in the petri dish, which was then positioned at the bottom of a beaker filled with 1000 g of water. The rotor was subsequently inserted into the beaker to generate water flow, maintaining a vertical distance of 80 mm between the rotor and the beaker bottom. The water was stirred at a speed of 350 rpm for 5 min. After stirring, the petri dish was removed and placed in an inclined position, and excess water was extracted using a 2.5 ml syringe needle. Finally, the mass of the remaining slurry was measured, and the washout resistance of the grout was calculated using Equation (1):

$$WR = 100 - \left(\frac{50 - AWSFG_R}{50} \times 100\right) \quad (1)$$

where $AWSFG_R$ is the mass of the remaining AWSFG grout.

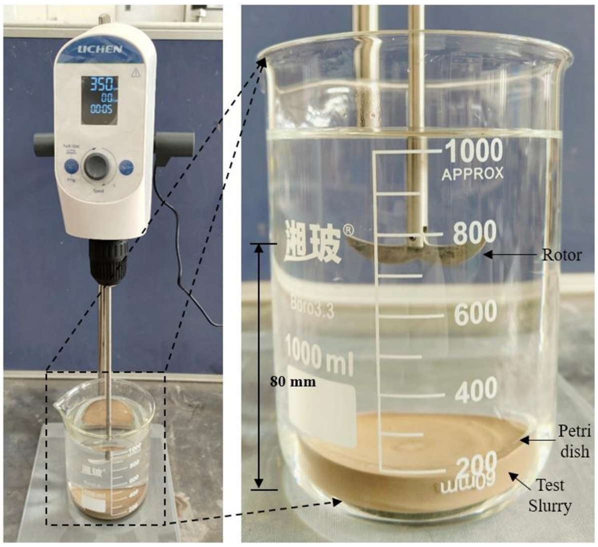

Fig. 4. Test setup for washout resistance.

2.2.4 Compressive strength test

The compressive strength of the AWSFG grout was evaluated in accordance with ASTM C1928/C1928M-23 [19]. Fig. 5 depicts the UCS specimen preparation and underwater curing procedure. Cubic molds with dimensions of 50 mm were positioned at a depth of 100 mm below the water surface prior to casting. Fresh AWSFG grout was poured into the molds through a funnel inserted 10 mm into the mold, while maintaining an approximate distance of 40 mm between the funnel outlet and the mold base, as shown in Fig. 5. The specimens were cured underwater at 30°C for 3 and 28 days. After the designated curing periods, UCS tests were conducted at a constant strain rate of 1 mm/min. To ensure repeatability, three specimens were prepared and tested for each mix at both curing ages, and the average UCS value was reported.

3 Results and discussion

3.1 Fluidity and turbidity

Fig. 6 illustrates the influence of activator modulus and Na_2O content on the fluidity and turbidity of AWSFG grout. At a constant Na_2O content, fluidity increased with increasing modulus. In contrast, at a fixed modulus, fluidity increased as the Na_2O content rose from 6% to 8% but decreased at 10% Na_2O across all modulus values.

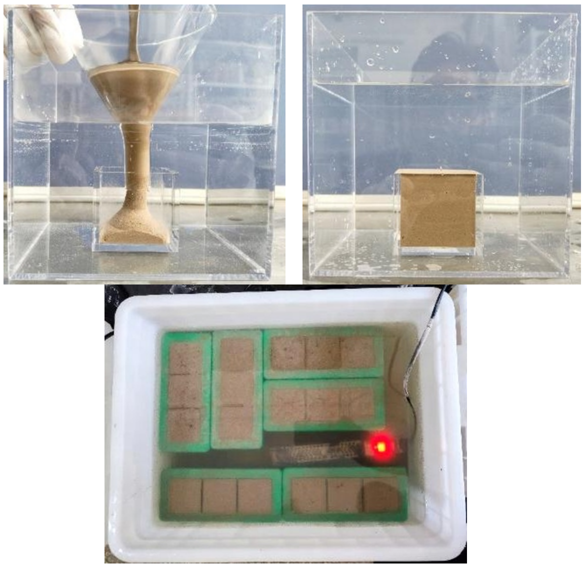
Fig. 5. UCS sample preparation process and curing.

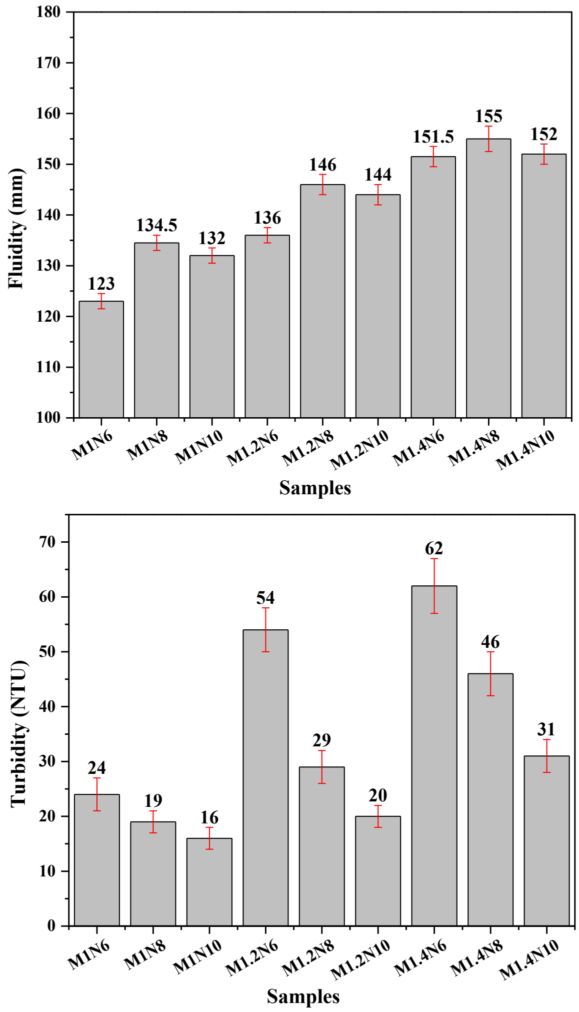

Fig. 6. Fluidity and turbidity of AWSFG grout at different modulus and Na_2O content.

With respect to turbidity, an increase in modulus at the same Na_2O content resulted in higher turbidity, whereas at a constant modulus, turbidity decreased with increasing Na_2O content. The observed increase in fluidity and turbidity with higher modulus is attributed to the reduced alkalinity of the grout. A higher modulus lowers alkalinity and slows aluminosilicate dissolution, thereby decelerating geopolymer hydration and promoting the accumulation of unreacted sodium silicate. Conversely, a higher Na_2O content enhances pore-fluid alkalinity and cohesiveness, thereby restricting slurry flow and reducing turbidity [20]. A lower modulus, combined with a higher Na_2O content, promotes the formation of primary CSH gel, resulting in reduced fluidity and turbidity, as observed for the M1N10 sample.

3.2 Initial and final setting time

Fig. 7 shows the effects of activator modulus and Na_2O content on the setting times of fresh AWSFG grout. For Na_2O contents ranging from 6% to 10%, both initial and final setting times generally increased with increasing modulus, except at a modulus of 1, where the final setting time decreased with increasing Na_2O content. At modulus values of 1.2 and 1.4, a pronounced increase in initial setting time was observed as Na_2O content increased from 6% to 8% and from 8% to 10%, respectively. In contrast, the final setting time exhibited only a marginal increase from 6% to 8% Na_2O, followed by a notable increase from 8% to 10%. At a modulus of 1, the final setting time decreased with increasing Na_2O content, showing a slight reduction from 6% to 8% and a more significant decrease from 8% to 10%. The prolonged setting times of AWSFG grout are mainly attributed to the strong adsorption of PAM on precursor particle surfaces and its high-water affinity. The adsorbed polymer layer retards aluminosilicate dissolution, while its water-binding capacity reduces the effective pore solution available for reaction. In addition, the increased grout viscosity restricts polycondensation of dissolved silicate and aluminate species, delaying geopolymer gel formation and thereby extending the setting times.

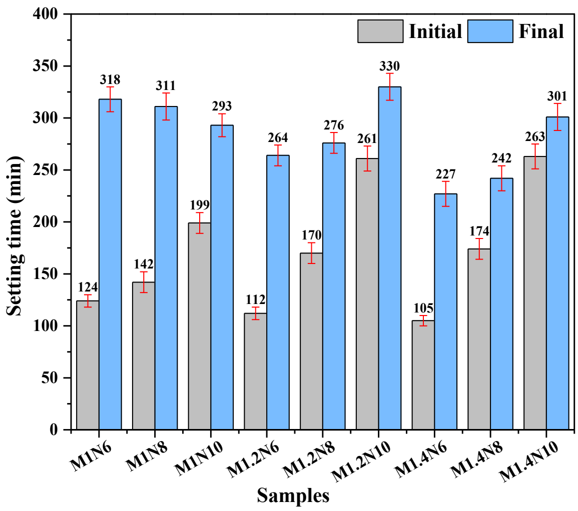

Fig. 7. Setting time of fresh AWSFG grout.

3.3 Washout resistance

Fig. 8 shows the washout resistance of fresh AWSFG grout at different modulus and Na_2O content. All the AWSFG grout samples exhibit washout resistance values of more than 99%, except the M1.4N10 sample. The higher washout resistance is attributed to the long-chain structure of PAM that flocculates and aggregates the particles of slurry into a cohesive network structure, improving the cohesion and viscosity characteristics of the fresh AWSFG grout and resulting in higher washout resistance [9]. The washout resistance of AWSFG grout was noted to be decreased with an increase in both modulus and Na_2O content. However, no significant effect of Na_2O content was pointed out at a modulus value of 1. A slight decrease was recorded at a 1.2 modulus value with increased Na_2O content. However, a notable decrement in washout was observed at a 10% Na_2O content and a modulus of 1.4.

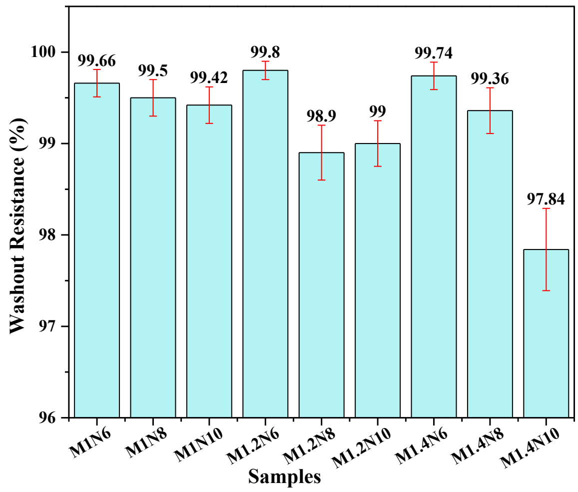

Fig. 8. Washout resistance of fresh AWSFG grout.

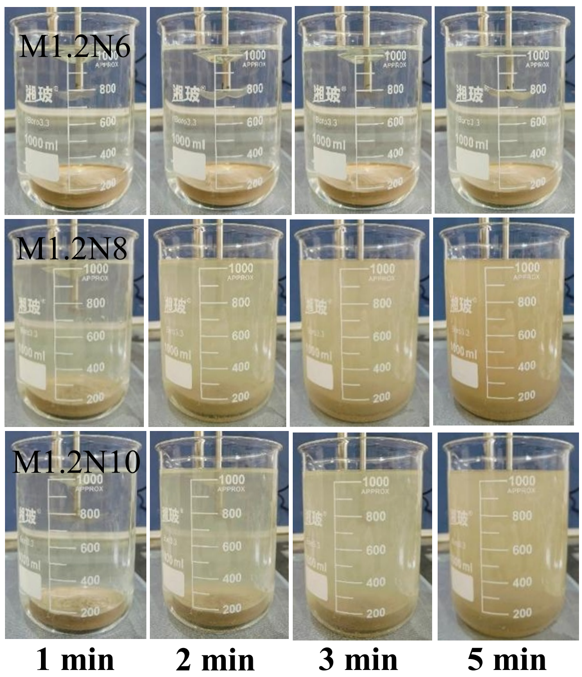

Fig. 9. Optical images of the anti-washout characteristics.

Fig. 9 displays the optical images of the washout resistance test. The optical images clearly show that the

M1.2N6 sample exhibited negligible washout loss and remained visually apparent even after 5 min of stirring. In contrast, the M1.2N8 and M1.2N10 samples became slightly turbid after 1 min of stirring and progressively muddier after 5 min, although their washout losses remained low at approximately 1%. The highest washout loss, 2.16%, was recorded for the M1.4N10 sample (Fig. 8). This behavior can be attributed to the higher modulus of the AWSFG grout, which lowers its alkalinity and suppresses the dissolution of aluminosilicates, thereby decelerating the geopolymerization process, promoting the accumulation of unreacted sodium silicate, and thereby reducing the grout's washout resistance.

3.4 Strength performance of AWSFG

Fig. 10 shows the UCS results of hardened AWSFG grout cast and cured underwater for 3 and 28 days of curing time. It is evident that both the activator modulus and Na_2O content plays a key role in governing the strength development of the grout. For all modulus values, UCS increased with Na_2O content. However, at a fixed Na_2O content, the UCS improved as the modulus rose from 1 to 1.2, but then showed a slight reduction at a modulus of 1.4 at both curing ages. Notably, a pronounced drop in the 3-day UCS was observed for the M1.4N10 sample.

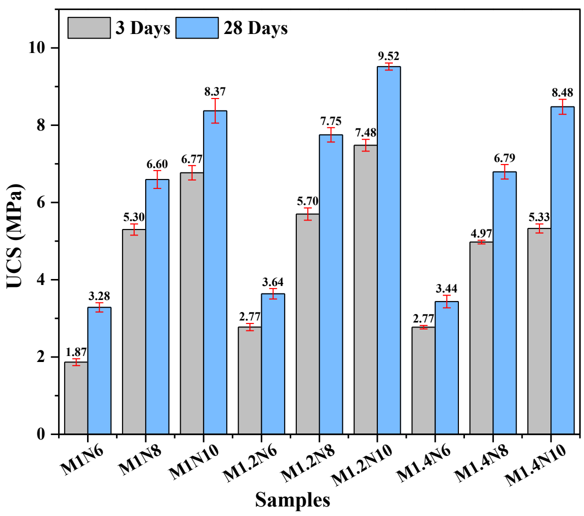

Fig. 10. UCS of hardened AWSFG grout.

The higher UCS values are mainly associated with the formation of NASH, CASH, and CSH gels, as well as ettringite (needle-like structures). An increase in Na_2O content raises the pH of the slurry, which accelerates aluminosilicate dissolution, enhances hydration, and promotes the formation of these binding phases, resulting in a denser microstructure and higher compressive strength [21, 22]. In contrast, mixes with higher modulus and reduced alkalinity exhibit lower pH, slower aluminosilicate dissolution, and delayed geopolymerization, leading to the accumulation of unreacted sodium silicate [13]. This mechanism explains the marked reduction in early-age UCS observed for the M1.4N10 sample.

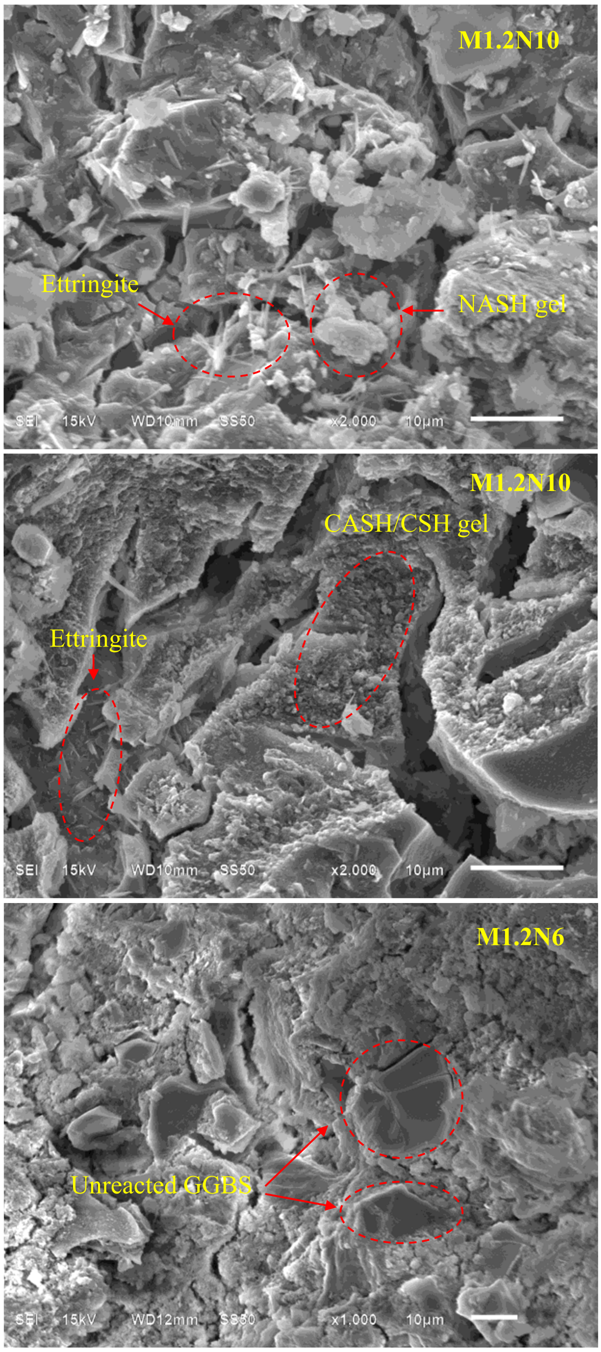

Fig. 11. SEM images of hardened AWSFG grout.

The UCS trends are further supported by SEM analysis. As shown in Fig. 11, the M1.2N10 sample cured underwater for 28 days exhibits abundant NASH and CASH/CSH gels, along with well-developed ettringite, which contribute to a dense microstructure and enhanced strength, primarily driven by NASH gel formation. Conversely, unreacted slag particles are evident in the M1N6, M1.2N6, and M1.4N6 mixes due to their lower Na_2O contents, consistent with their comparatively lower UCS values.

3.5 Limitations and future scope

Although this study provides valuable insights into the development of anti-washout grout, several limitations could be addressed in future research. The results were obtained under laboratory conditions using distilled water. In addition, only a small dosage of PAM was adopted, and variations in its content may further enhance washout resistance. It is also well established that the fresh and hardened properties of cementitious materials in seawater exhibit more complex and distinct behavior compared to those in distilled water or freshwater. Therefore, the influence of seawater on the strength and durability of AWSFG grout should be systematically investigated in future studies. Moreover, the dredged river soil used in this study is predominantly silty; comparative investigations involving other soil types, such as sandy or clayey soils, would be valuable to assess their suitability and performance as anti-scouring materials. The field implementation of the proposed grout should be investigated through pilot-scale testing and numerical simulations. In addition, at this stage, the study is primarily focused on developing sustainable geopolymer grout. However, a comparison with conventional concrete-based anti-scour solutions will provide a better perspective of the proposed geopolymer grout.

4 Summary and conclusions

This study investigates a geopolymer-based anti-washout grout to prevent the scouring around the foundations of marine structures with minimal environmental impacts. A sustainable AWSFG grout was developed using soil as the primary material, FA and GGBS as precursors, activated with alkali solutions, and modified with a small dosage of cationic PAM. The effects of activator modulus and Na_2O content on the fresh and hardened properties of the grout under underwater conditions were systematically investigated. Based on the experimental results, the following conclusions can be drawn:

1. The activator modulus and Na_2O content jointly govern the rheological behavior of AWSFG grout. The fluidity increased with increasing modulus at a fixed Na_2O content, while an optimum Na_2O content of 8% yielded the highest fluidity across all modulus values. Excessive Na_2O content (10%) reduced fluidity due to increased pore-fluid alkalinity and cohesiveness.
2. Turbidity and anti-dispersion performance were strongly influenced by activator modulus and Na_2O content. Higher modulus values led to increased turbidity, whereas increasing Na_2O content at a fixed modulus reduced turbidity.
3. The incorporation of 0.1% PAM effectively enhanced particle cohesion, resulting in excellent anti-washout performance, with washout resistance exceeding 99% for most mixes, except the sample with higher modulus and higher Na_2O content (M1.4N10).
4. The setting time behavior of AWSFG grout was sensitive to both modulus and Na_2O content. In general, higher modulus values prolonged initial and final setting times, particularly at higher Na_2O contents. The delayed setting is mainly attributed to the adsorption of PAM on precursor surfaces, its water-retention capacity, and the associated increase in grout viscosity, which collectively slow aluminosilicate dissolution and geopolymer gel formation.
5. Under underwater casting and curing conditions, the UCS of AWSFG grout increased with increasing Na_2O content for all modulus values. At a constant Na_2O content, strength improved as the modulus increased from 1.0 to 1.2, but decreased slightly at a modulus of 1.4. A notable reduction in early-age strength was observed for the M1.4N10 mix, highlighting the adverse effect of excessive modulus on early geopolymerization.
6. Microstructural analyses confirmed that higher strength was associated with the co-existence of ettringite, NASH, CASH, and CSH gels, which together formed a dense and well-interlocked matrix. Moreover, samples with lower Na_2O content exhibited unreacted slag particles, which accounted for their comparatively lower UCS.
7. Among all formulations, the M1.2N10 sample demonstrated the most balanced performance in terms of fluidity, setting time, washout resistance, and strength development, making it the optimum composition for underwater anti-scour applications.

In conclusion, the AWSFG grout developed in this study exhibits remarkable underwater stability and mechanical performance while significantly reducing cement use. By effectively utilizing dredged sediments and industrial by-products, this grout offers a low-carbon, cost-effective, and environmentally sustainable solution for offshore scour protection and underwater ground improvement applications.

This research is supported by the Changji Prefecture Regional Collaborative Innovation Special Program (2025X02), and Shenzhen Science and Technology Program (SZXJP20230703093002005).

All data generated or used during the study appear in this published article.

Deepak Patwa: Conceptualization, Methodology, Data Curation, Investigation, Formal analysis, Writing-original draft. Sang Zihan: Data Curation. Deepesh Bansal: Methodology, Writing-review and editing. Kai Yao: Supervision.

References

1. F. Geng, W. Yang, S. Nadimi, and Z. Hu, Development and prediction of scour around offshore wind turbine monopile foundations in ebb and flow tides, Ocean Eng. **311**, 118905 (2024). https://doi.org/10.1016/j.oceaneng.2024.118905
2. F. Sha, J. Xu, S. Gu, Y. Dong, and W. Xiao, A review on fluid-sediment and foundation-sediment coupling mechanisms and anti-scour countermeasures, Mar. Struct. **103**, 103843 (2025).https://doi.org/10.1016/j.marstruc.2025.103843
3. R. Hu, Y. Lu, H. Leng, H. Liu, and W. Shi, A novel countermeasure for preventing scour around monopile foundations using Ionic Soil Stabilizer solidified slurry,

Appl. Ocean Res. **121**, 103121 (2022).https://doi.org/10.1016/j.apor.2022.103121

4. H. Kang, X. Han, X. Wang, Z. Cai, Y. Guan, and W. Wang, Improving the scour-resistance performance of for offshore wind turbines: Experimental and computational fluid dynamics studies on macro and micro characteristics, Constr. Build. Mater. **444**, 137762 (2024).https://doi.org/10.1016/j.conbuildmat.2024.137762
5. X. Li, Z. Zhu, R. Liu, C. Zhang, Q. Zhang, S. Li, and M. Chen, Preparation of anti-washout cement-stabilized marine soft clay for scouring protection of wind power pile foundations, Mar. Georesources Geotechnol. **42**, 506 (2024).https://doi.org/10.1080/1064119X.2023.2204335
6. G. Habert, C. Billard, P. Rossi, C. Chen, and N. Roussel, Cement production technology improvement compared to factor 4 objectives, Cem. Concr. Res. **40**, 820 (2010).http://dx.doi.org/10.1016/j.cemconres.2009.09.031
7. S. Rios, N. Cristelo, A. Viana da Fonseca, and C. Ferreira, Structural Performance of Alkali-Activated Soil Ash versus Soil Cement, J. Mater. Civ. Eng. **28**, 1 (2016).https://doi.org/10.1061/(ASCE)MT.1943-5533.0001398
8. S. Singh, A. Kumar, and T. G. Sitharam, Experimental study on strength, durability, hydraulic and toxicity characteristics of soil treated with mine tailings based geopolymers for sustainable road subgrade application, Constr. Build. Mater. **414**, 134894 (2024).https://doi.org/10.1016/j.conbuildmat.2024.134894
9. X. Sun, W. Liu, X. Chen, S. Wu, G. Chen, Y. Bi, and Z. Chen, Sustainable solutions: Transforming waste shield tunnelling soil into geopolymer-based underwater backfills, J. Clean. Prod. **445**, 141363 (2024).https://doi.org/10.1016/j.jclepro.2024.141363
10. A. Noushini and A. Castel, Performance-based criteria to assess the suitability of geopolymer concrete in marine environments using modified ASTM C1202 and ASTM C1556 methods, Mater. Struct. **51**, 146 (2018).http://link.springer.com/10.1617/s11527-018-1267-z
11. D. Patwa, Z. Sang, S. Zhang, K. Yao, Z. Liu, L. Liu, H. Cao, and Z. Yao, Sustainable anti-washout geopolymer grout from soil-fly ash-GGBS for scour protection of offshore structures under in-situ conditions, J. Sustain. Cem. Mater. **15**, 408 (2026).https://doi.org/10.1080/21650373.2025.2569893
12. D. Patwa, K. Yao, Z. Sang, Z. Liu, L. Liu, and Z. Yao, Strength, Flow, Setting, and Antiwashout Performance of Alkali-Activated Soil-Fly Ash-GGBS Grout for Scouring Protection of Marine Structures, J. Mater. Civ. Eng. (2026).10.1061/JMCEE7.MTENG-22813
13. H. X. Chen, Q. P. Xue, Z. P. Ma, L. Gao, and S. J. Feng, Experimental study on barrier performance and durability under dry-wet cycles of fly ash based geopolymer cutoff wall backfill, Constr. Build. Mater. **368**, 130415 (2023).https://doi.org/10.1016/j.conbuildmat.2023.130415
14. O. Burciaga-Díaz, L. Y. Gómez-Zamorano, and J. I. Escalante-García, Influence of the long term curing temperature on the hydration of alkaline binders of blast furnace slag-metakaolin, Constr. Build. Mater. **113**, 917 (2016).http://dx.doi.org/10.1016/j.conbuildmat.2016.03.111
15. X. Ji, Z. Wang, X. Wang, X. Zhao, H. Zhang, and T. Zhang, Microstructures and properties of alkali-activated slags with composite activator: Effects of Na2O equivalents, J. Clean. Prod. **450**, 141754 (2024).https://doi.org/10.1016/j.jclepro.2024.141754
16. A. M. Rashad, S. R. Zeedan, and A. A. Hassan, Influence of the activator concentration of sodium silicate on the thermal properties of alkali-activated slag pastes, Constr. Build. Mater. **102**, 811 (2016).https://doi.org/10.1016/j.conbuildmat.2015.11.023
17. GB/T 8077-2023, *Methods for Testing Uniformity of Concrete Admixtures*, (2023).https://www.chinesestandard.net/PDF/English.aspx/GBT8077-2023
18. ASTM C191-21 (2021), Standard Test Methods for Time of Setting of Hydraulic Cement by Vicat Needle, ASTM Int. **1**, 5 (2021).10.1520/C0191-21.2
19. ASTM C1928/C1928M-23, Standard Test Method for Compressive Strength of Alkali Activated Cementitious Material Mortars (Using 2-in . [50 mm] Cube Specimens), ASTM Int. West Conshohocken, PA United States (2023).10.1520/C1928
20. S. Samantasinghar and S. P. Singh, Fresh and Hardened Properties of Fly Ash–Slag Blended Geopolymer Paste and Mortar, Int. J. Concr. Struct. Mater. **13**, 1 (2019).
21. S. Fang, E. S. S. Lam, B. Li, and B. Wu, Effect of alkali contents, moduli and curing time on engineering properties of alkali activated slag, Constr. Build. Mater. **249**, (2020).https://doi.org/10.1016/j.conbuildmat.2019.117481
22. W. C. Wang, H. Y. Wang, and H. C. Tsai, Study on engineering properties of alkali-activated ladle furnace slag geopolymer, Constr. Build. Mater. **123**, 800 (2016).http://dx.doi.org/10.1016/j.conbuildmat.2016.07.068